Synthesis of carbon quantum dots and Fe-doped carbon quantum dots as fluorescent probes via one-step microwave process for rapid and accurate detection of Diclofenac sodium

Arsalan Gholipour
Babol Noshirvani University of Technology

Hamid Emadi
University of Mazandaran

Mohsen Jahanshahi (✉ mjahan@nit.ac.ir)
Babol Noshirvani University of Technology

Research Article

Abstract

In the current study, the carbon quantum dots (CDs) were synthesized through a facile, rapid, and one-step microwave method using citric acid monohydrate and urea. The as-prepared CDs were spherical with diameters of 3−4 nm and displayed bright blue fluorescent under an excitation wavelength of 360 nm. Also, the as-prepared CDs had various properties, including favorable solubility in water, different functional groups, significant stability in various environmental conditions, and excellent optical performance. The results indicated that the CDs could be applied as a fluorescent probe for reliable and accurate detection of Diclofenac sodium (DFS) based on the enhancement of their native fluorescent intensity (turn-on). The emission spectra of the as-prepared CDs were strengthened gradually when the DFS concentration increased from 5 to 300 µM. In addition, the linear relationship was fabricated over the concentrations range of 5-300 µM for DFS with the detection limit of 2.33 µM. Furthermore, the findings showed that Fe doped CDs (Fe-CDs) like CDs have a good ability to detect various concentrations of DFS in the wide range of 5-300 µM.

Introduction

The Carbon quantum dots (CQDs or CDs) are the most durable allotropes of carbon-based nanomaterials, and their sizes are usually less than 10 nm [1]. These luminescent semiconductor carbon nanoparticles (CDs) are a unique class of carbon nanomaterials that have been used widely in various applications such as bio-sensing and bio-imaging [2], carrier vehicles for drug and gene delivery [3], light-emitting diodes and fluorescent probe [4], photocatalytic activity [5], analyte detection and probe contaminants in water environment [6], and storage devices [7] due to their special properties such as high photostability, low toxicity, biocompatibility, high-water solubility, strong fluorescence lifetime and tunable excitation and emission wavelength [8, 9].

According to the specific characteristics of CDs and various synthesis methods, and a broad range of inexpensive raw materials as precursors [10], many researchers around the world have interested in using these materials as fluorescent probes based on "turn-off" or "turn-on" fluorescence in medical and biological applications for detecting different kinds of analytes. Zhao et al. prepared CDs by hydrothermal method via pine wood as carbon precursor for selective and sensitive detection of Fe^{3+}. The limit of detection (LOD) was 355.4 nM, and the fluorescence (FL) intensity of the CDs gradually decreased when the concentration of Fe^{3+} increased [11]. In another research, Hu et al. synthesized CDs combined with magnetic nanoparticles (MNPs) by orange peel as a carbon source via the simple and green one-step microwave-assisted pyrolysis for specific detection of Escherichia coli O157: H7 (E. coli) in milk. The CDs displayed bright green fluorescence under an excitation wavelength of 420 nm with an average size of 4.2 nm. The FL intensity of the CQDs-MNPs decreased with the addition of E. coli [9]. Despite the great variety of synthesized CQDs, the main drawback of their applications is their relatively low quantum yields. In this sense, doping is a widely used approach to improve the quantum yield, photoluminescent performance, active sites of CDs, and to change their internal electronic structure [12, 13]. Zhang et al. used citric acid monohydrate and boric acid as precursors to prepare boron-doped CDs (B-CDs) through

one-step hydropyrolysis for sensitive detection of amoxicillin. The as-prepared B-CDs had a narrow diameter range and a quantum yield of 30.85%. The LOD was 0.825 μM, and the emission spectra were strengthened gradually when the amoxicillin concentration increased from 0 to 429.12 μM [14]. It is important to note that the selection of carbon-containing precursors and the management of synthesis conditions have a significant effect on the luminescence mechanism of CDs [15]. Therefore, it is important to choose a suitable raw material and the best synthesis method for producing carbon dots with unique properties.

Diclofenac sodium (DFS) (sodium [o-(2,6-dichloroanilino) phenyl] acetate), as a potent non-antibiotic/antibacterial agent, is safe, popular, and widely used around the world. DFS can be absorbed very well after administration orally and is well known as a non-steroidal anti-inflammatory drug (NSAIDs) that has antipyretic, analgesic, anti-inflammatory, and anti-rheumatic properties [16]. Prolonged use of DFS may have undesirable side effects, such as heart attack and stroke [17]. Until now, many different methods such as high-performance liquid chromatography (HPLC) [18], liquid chromatography-Tandem mass spectrometry (LC-MS/MS) [19], and gas chromatography-mass spectrometry (GC-MS) [20] have been established to determine various concentrations of DFS in different systems. Although, these techniques are common and sometimes are sensitive with a suitable LOD, some drawbacks such as time-consuming, high cost, need for chemical reagents, and pre-treatment steps prior to the analysis limited their use in biological applications. Keeping in mind, according to the huge commercial demand in medical, biomedical, and pharmaceuticals applications and the potential adverse effects of DFS on human, animal, and environmental health, urgent efforts are essential more than ever to consider a facile, selective, fast, sensitive, and cost-effective techniques for measurement and detection of this drug in various types of systems even in low concentrations. Hence, interest has been attracted towards the methods that have excellent properties, including high sensitivity and selectivity, fast response, facile operation, cost-effectiveness, the possibilities of miniaturization, and on-site-applicable. In this work, a fast and facile strategy was declared to synthesize CDs with various properties via a one-step microwave approach without adding additional agents. The optical and physicochemical properties of the as-prepared CDs were investigated by detailed analysis. The results indicated that CDs and Fe-CDs have good ability as fluorescent probes to detect various concentrations of DFS in different environments and real samples.

Experimental

Chemicals and Reagents

All chemicals which have been used in this paper, were with high purity, without any further purification, and were in analytical grade. Citric acid monohydrate, Urea, Tetracycline (Tet), Carvedilol (Car), Metformin (Met), Loratadine (Lor), Naproxen (Nap), Aspirin (Asp), Sodium chloride (NaCl), and Ethanol were purchased from Sigma-Aldrich Company (St. Louis, United States). Furthermore, Sodium hydroxide (NaOH), Hydrochloric acid (HCl), Methanol, and $FeCl_3.6H_2O$ were prepared from Merck Company

(Darmstadt, Germany). In addition, Diclofenac sodium (DFS), Indomethacin (Ind), Amoxicillin (Amo), Ciprofloxacin (Cip), Methionine (MET), Tyrosine (Tyr), $MgCl_2$, and $AlCl_3$ were obtained from Aladdin Biochemical Technology Company (Shanghai, China). Double-distilled water was used in all experiments.

Instrumentations and Characterizations

The particle size distribution histogram and morphologies of the samples were acquired by High-resolution transmission electron microscopy (HRTEM) images that were carried out on a FEI TEC9G20 electron microscope at an operating voltage of 200 kV (USA). By dropping the particle samples onto carbon-coated copper grids and allowing them to evaporate the excess solvent by drying at room temperature, the HRTEM analysis was obtained. The UV-Vis absorption spectra were recorded on a UV-3600 spectrometer (Shimadzu, Japan). Photoluminescence spectra (PL) of the samples were obtained with a FP-8300 fluorescence spectrophotometer (JASCO, Japan). Both excitation and emission slits were fixed at 10 nm. Fourier transform infrared spectroscopy (FT-IR) and X-ray Photoelectron Spectroscopy (XPS) were revealed via Fourier transform infrared spectrometer (Vertex 70, Bruker, Germany) and X-ray photoelectron spectrometer (ESCALAB Xi+, Thermo Fisher Scientific, USA) to investigate the functional groups and surface chemical compositions of the as-prepared CDs, respectively. The X-ray diffraction (XRD) pattern was collected on a D-500 XRD (Siemens, Munich, Germany) to demonstrate the crystal structure of as-prepared CDs. By applying Scanning electron microscopy (SEM, JSM-7900F, JEOL, Japan) with energy dispersive spectroscopy (EDS), the SEM images and EDS spectrum of the sample were collected. Raman spectrum of CDs was obtained by LabRAM HR800 laser confocal Raman spectrometer (HORIBA Scientific Jobin, France). The microwave-assisted reaction was done in a microwave oven with a tunable output power (100–1000 w), tunable time (1 s – 29 min: 59 s), tunable pressure (maximum working pressure is 35 atm), tunable temperature (maximum working temperature is 235°C), and a 2450-MHz microwave frequency, 1500 W, WX-4000 (Preekem Scientific Instruments, Shanghai, China). It should be noted that all optical measurements were performed at room temperature under ambient conditions.

Preparation of Fluorescent CDs

The fluorescent CDs were synthesized using citric acid monohydrate and urea as precursors via a simple, rapid, and one-step microwave pyrolysis method. Briefly, 3 gr of citric acid monohydrate and 3 gr of urea were dissolved in 10 ml ultrapure water and stirred until a transparent and homogeneous solution was achieved. Then, the mixture was irradiated by a microwave oven (750 W) for 150 s. After completion of the reaction, the mixture was cooled to room temperature. To separate large particles and collect highly fluorescent carbon dots, the brownish-black solid was centrifuged at 12000 rpm for 10 min and washed 4 times by water and mixture of ethanol and water. Afterward, the CDs solution was filtered through a 0.22 μm micropore membrane. For further purification and separation of unreacted molecules, and to remove excess solvents, CDs powders were dried under a vacuum oven at 60°C (1 hr). As a result, CDs powders were obtained by evaporation, re-dispersed in deionized water, and stored at 4°C for further use.

Diclofenac Sodium (DFS) Sensing

To investigate the sensitivity of as-prepared CDs towards DFS, different concentrations of DFS (5, 10, 20, 40, 50, 60, 100, 120, 140, 180, 220, 260, and 300 μM) were prepared in methanol. The reaction was allowed to take place at room temperature for 10 min, then the changes of fluorescence emission spectra with excitation wavelength at 360 nm were measured from 300 to 700 nm to assay the sensitivity of as-prepared CDs towards DFS. The concentration of CDs was adjusted to 5 μg.ml^{-1} in all measurements.

Results And Discussion

Structural Characterization of CDs

The crystallinity of CDs was investigated by XRD. Figure 1a displays the XRD pattern of CDs with a broad diffraction peak located at 23.54°, which corresponds to the (100) lattice spacing of the carbon-based materials and indicates the presence of graphite lattice in the structure of as-prepared CDs. Furthermore, the XRD pattern probably can introduce the amorphous nature and disordered structure of CDs [21, 22]. Also, Raman analysis was applied to investigate the graphitic nature of the CDs [23, 24]. The Raman spectrum of CDs indicated that two main peaks located at 1362 cm^{-1} (D-band) and 1583 cm^{-1} (G-band), which are attributed to the sp^3 and sp^2 hybridized carbon in the structure of as-prepared CDs, respectively (Fig. 1b) [25]. By observing an I_D/I_G ratio ($\approx$0.86), it can be assumed that there are some defects in the structure of as-prepared CDs.

To evaluate the surface functional groups of as-prepared CDs, the FTIR spectrum was performed (Fig. 2). The broad peak at 3435 cm^{-1} corresponds to the bending vibrations of the -OH groups. The peaks located at 2072 cm^{-1} and 3183−3383 cm^{-1} belong to the stretching vibrations of the N-H groups. Moreover, the peaks at 2847, 1720, 1639, 1273, 1107, and 1086 cm^{-1} were attributed to vibrations of C-H, C = O, C = O/C = N, C-N, C-O-C, and C-O groups, respectively [26−28]. These results indicated that abundant oxygen-containing groups such as carboxylic and hydroxyl groups existed on the surface of CDs. The existence of these groups in the structure of CDs has an excellent effect on their stability and hydrophilicity in the various systems.

In addition, the synthesized CDs were analyzed by SEM, and the acquired image illustrated a rough dispersed state of CDs. EDS spectrum of as-prepared CDs described the existence of three main elements including carbon, oxygen, and nitrogen in the structure of CDs, as shown in Fig. 3a. In other words, carbon, nitrogen, and oxygen elements were accounted for about 51, 27, and 22% of the structure of the synthesized CDs, respectively. The elemental mapping showed that these elements are well distributed in the structure of CDs, which was corresponded to other researches (Fig. 3b) [29]. In addition, the surface chemical composition of the as-prepared CDs was confirmed by XPS measurement (Fig. 4a). The full range XPS spectrum revealed that the as-prepared CDs mainly consist of carbon (C1s, 284.8eV, 50.98%), nitrogen (N1s, 399.55eV, 26.79%), and oxygen (O1s, 532.17eV, 22.23%) which was completely consistent with the EDS spectrum. The high-resolution C1s spectra of CDs indicated three peaks located at 284.3 eV, 288.1 eV, and 288.8 eV, which are attributed to C-C/C = C, C = N, and C = O groups, respectively (Fig. 4b).

On the other hand, the existence of different peaks in the C1s spectrum indicates the presence of carbon in various chemical environments. The N1s high-resolution spectra of CDs exhibited two peaks located at 399.4 eV and 401.8 eV, attributed to pyrrolic N and N-H bonds, respectively (Fig. 4c). In addition, the peaks at 531.5 eV and 533.2 eV corresponded to the C = O and C-O groups which could be clearly observed in the O1s high-resolution spectra of as-prepared CDs (Fig. 4d) [30–32]. The results obtained from FTIR and XPS analyses demonstrated that the as-prepared CDs inherited amounts of oxygen and nitrogen-containing groups on their surfaces. The diverse functional groups on the surface of as-prepared CDs equipped these fluorescent materials with various features such as good water solubility and excellent optical properties, and provide the possibility of using them in various fields.

The histogram and morphologies of the as-prepared CDs were evaluated by HRTEM images. As shown in Fig. 5a, the HRTEM Images proved that the as-prepared CDs were spherical and well dispersed in different resolutions. Furthermore, the HRTEM images indicated that the as-prepared CDs had suitable crystalline lattice spacing ($\approx$0.24 nm), which could correspond to the lattice constant of graphite (graphitic carbon) and indicated the graphitic nature of CDs [33–36]. Also, the size distribution of particles ranged from 1 to 6 nm, and the average size of monodisperse CDs was around 3.6 nm by measuring the diameters of 50 particles (Fig. 5b).

Optical Properties of CDs

The optical properties of as-prepared CDs were investigated by UV-Vis absorption and photoluminescence spectra. As shown in Fig. 6a, the as-prepared CDs exhibited one weak peak located at 236 nm and two strong absorption peaks located at 275 nm and 345 nm. The strong peaks at 275 nm and 345 nm can be ascribed to the π-π* transitions of the sp^2-hybridized carbon bonds (C = C) [37] and the n-π* transitions of the C-O and C = O structures in the CDs, respectively [38]. Furthermore, the emission spectrum of CDs is usually strongly dependent on the excitation wavelength. Therefore, assessing the dependence or non-dependence of the emission spectrum of CDs than the excitation wavelength is one of the important points that should be considered. Hence, the emission spectrum of CDs was evaluated at diverse excitation wavelengths ranging from 320 to 380 nm with a 10 nm increment. It was observed that by increasing excitation wavelength from 320 to 380 nm, the emission spectrums moved to a longer wavelength, while their intensity decreased when the excitation wavelength was more than 360 nm. As shown in Fig. 6b, the best emission intensity was observed at 360 nm. Therefore, with the optimal excitation wavelength at 360 nm, the as-prepared CDs showed the strongest peak at 445 nm (Fig. 6c). These excitation wavelength-dependent fluorescence characteristics of CDs can be attributed to the various size of nanoparticles in the samples (quantum effect) and the diverse functional groups that exist on the surface of CDs [39, 40].

To verify the ability of CDs as a fluorescent probe, the as-prepared CDs were investigated to detect DFS in diverse concentrations. Here, different concentrations of DFS from 5-300 µM (5, 10, 20, 40, 50, 60, 100, 120, 140, 180, 220, 260, and 300 µM) were prepared in detection system. Figure 7a shows the fluorescence spectra of as-prepared CDs in the presence of various concentrations of DFS with excitation

wavelength at 360 nm. The fluorescence emission spectra of the CDs-DFS detection system can be changed with different DFS concentrations. On the other hand, the results indicated that the fluorescence spectra of the sensing system were enhanced gradually with increasing DFS concentration. It should be noted that the electrons can reside in various energy levels. However, the tendency of electrons is located in lower energy levels (steady state). Upon excitation, electrons move from a lower energy level (valence band) to a higher energy level (conduction band). As a result, a positively charged hole in one of the levels (valence band) and a free electron in the other level (conduction band) are created. Therefore, exciton (a bound electron-hole pair) is formed, and fluorescence is produced by the combination of electron and hole [41–43]. However, due to the introduction of various analytes, strong interactions between the external electrons of the fluorescent substance and the desired analyte are formed, which lead to the occupation of holes and prevent electron-hole recombination on the surface of CDs [44]. Thus, a significant decrease in the FL intensity of the CDs occurs. In the case of DFS, the process was different. As we mentioned, electrons are unstable in the excited state and tend to quickly return to their stable state. When the electrons intend to return from the excited state to the ground state, they must give back their excess energy in the form of radiation or non-radiation. The DFS can increase the fluorescence properties of as-prepared CDs by decreasing their non-radiative transitions and improving the defects [14, 45, 46]. As a result, the as-prepared CDs can be used as a fluorescent probe for reliable and accurate detection of DFS based on the enhancement of the FL intensity. Furthermore, the changes in the FL intensity of as-prepared CDs ($F = F\text{-}F_0$, where F and F_0 are the FL intensities of as-prepared CDs in the presence and absence of DFS, respectively) had a good linear regression correlation with the concentrations of DFS in the range of 5-300 μM (Fig. 7b). The linear equation for DFS was $F = 0.0027$ $C_{DFS} + 0.0081$, and the correlation coefficient was $R^2 = 0.9996$. The LOD was calculated to be 2.33 μM according to the 3σ/K (S/N = 3).

The Stability of CDs Versus Diverse Environmental Conditions

The stability of CDs in various environmental conditions is a vitally important parameter for their better performance and efficiency in different fields. Therefore, the fluorescence properties of as-prepared CDs were evaluated under harsh and diverse conditions. To evaluate the photostability, the CDs solution is placed under a 360 nm UV lamp at different irradiation times. As shown in Fig. 8a, the FL intensity of CDs shows only a negligible decrease even after 1 hour of continuous irradiation. The result proves the excellent photostability of as-prepared CDs. To evaluate the storage stability of CDs, the effect of the storage time on the FL intensity of CDs was explored. As demonstrated in Fig. 8b, more than 85% of the initial fluorescence is still maintained even after 60 days, indicating the strong resistance of CDs to photobleaching. Furthermore, the effects of pH value and ionic strength of the solution on the FL intensity of CDs were also investigated. As exhibited in Fig. 8c, the maximum FL intensity was observed at pH 6–7, which indicates that neutral conditions are more suitable for fluorescence detection. Both decreasing the pH value from 7 to 1 and increasing the pH value from 7 to 13 led to decrease in the FL intensity of CDs. Such pH-dependent fluorescence behavior can be attributed to the protonation or deprotonation of

functional groups that are present on the surface of CDs [47, 48]. It is worth mentioning that while the pH value increased from 1 to 13, the emission peak of the CDs was gradually changed. Although some mechanism models such as change of energy level and protonation and deprotonation have been explored in response to pH, a specific mechanism for justification of this behavior will be necessary for the future to analyze the structure and optical properties of CDs well. The stability of nanoparticles in high ionic strength media is another important factor that should be considered to evaluate the performance of nanomaterials. For this aim, the FL intensity of CDs was measured in a solution including various concentrations of NaCl. As illustrated in Fig. 8d, the FL intensity of CDs had no obvious change even at a high ionic strength of 3.0 M, which perfectly indicates that CDs could be suitable for any system, even in environments containing different salt solutions. These findings demonstrate that the as-prepared CDs are highly stable even under complicated and diverse physiological conditions. As a result, the obtained CDs have great potential and numerous advantages for practical applications.

The CDs-Based Test Papers for Detection of DFS

Nanocelluloses (NCs) is considered as the natural polymers with great characteristics such as favorable thermal stability, high surface area, excellent mechanical properties, and biocompatibility. Therefore, the combination of CDs and NCs in different fields may lead to wonderful results. To evaluate the capability of CDs as a fluorescent probe in various environments, the as-prepared CDs and different concentrations of DFS were fixed on the paper (NCs), and their color changes were investigated under UV irradiation. As shown in Fig. 9, when there was no DFS, the test paper displayed blue fluorescent under UV irradiation. After that, by increasing the concentration of DFS, the color of the test paper was gradually enhanced. In other words, the as-prepared CDs can be applied as a fluorescent probe for detection of various concentrations of DFS on the paper. Therefore, according to the diverse analyses, it can be concluded that the as-prepared CDs have numerous properties such as high-water solubility, different functional groups, and excellent optical performance which suggest that there will be great prospects for the as-prepared CDs as fluorescent probe in the future.

Selectivity of CDs Towards DFS

In addition, to optimal optical performance, an excellent fluorescent probe should also have good selectivity toward the desired target. Actually, selectivity is an important parameter that affects the performances of the as-prepared CDs. Same concentration of 10 different drugs including Tet, DFS, Cip, Car, Amo, Ind, Met, Lor, Nap, Asp, 3 metal ions such as Na^+, Mg^+, Al^{3+}, and 2 amino acids including MET and Tyr were separately added at a concentration of 100 μM to the obtained CDs solution to evaluate the fluorescence response of CDs towards different interfering substances. As indicated in Fig. 10, no obvious change in the FL intensity was observed for CDs with the addition of 100 μM drugs, metal ions, and amino acids, whereas a significant increase in FL intensity was obtained for DFS. In addition, the structure of the Ind, Nap, and Asp are similar to DFS. Therefore, as shown in Fig. 10, slight interferences were observed for FL intensity of the CDs solution after addition of these substances. The results showed that the mentioned substances which exist in the solution cannot have a significant effect on the optical

detection of DFS, which indicates that the proposed method can be applied as an excellent fluorescent probe for the sensitive and selective detection of DFS.

Analysis of Real Samples

The ability of the proposed approach in the practical applications was evaluated to investigate the reliability and sensitivity of the method towards DFS. For this aim, two different real samples (tap water and mineral water) were selected. To purify samples, the impurities and undesirable particles (large particles) were separated by centrifuging at 10,000 rpm for 18 min and further filtered through a 0.22 μm filter membrane. Standard recovery experiments were applied for DFS detection in the water samples at two different concentration levels. Accordingly, a constant value of real samples (6ml) were spiked with DFS working solution to obtain final concentrations of 5 and 10 μM. The results from Table 1 implies that the average recovery of DFS was more than 97% with an appropriate RSD (%) in both real samples. These findings indicate that the designed CDs-based fluorescent probe is a completely promising approach to detect the different concentrations of DFS in various environments and real samples.

Table 1
Recovery values and precision of DFS in water samples

Sample	DFS added (μM)	DFS found (μM)	Recovery (%)	RSD (%)
Tap water	0.00	N. D.*	-	-
	5.00		95.4	2.27
	10.00	4.77	96.6	1.69
		9.66		
Mineral water	0.00	N. D.*	-	-
	5.00		97.8	1.123
	10.00	4.89	98.3	0.84
		9.83		
N.D.* = Not detected				

The Effect of Fe^{3+} on The Optical Characteristics of As-Prepared CDs

To improve the sensitivity of the sensor, CDs were doped with Fe^{3+} ions (by microwave irradiation, 750 W, 150 s) and their fluorescence changes after addition of DFS were investigated. Figure 11a illustrates the fluorescent spectra of Fe-CDs in the presence of different concentrations of DFS. As can be seen, by

increasing concentrations of DFS from 5 to 300 µM, the FL intensity of Fe-CDs increases. By comparing Fig. 7a& 11a, it can be concluded that the fluorescent of Fe-CDs is decreased significantly compared to the CDs. The mechanism of quenching the FL intensity of Fe-CDs can be considered based on the interactions formed between the oxygen/nitrogen-containing groups on the surface of CDs with Fe^{3+} ions. As mentioned, the surface of CDs contains different functional groups such as -OH, N-H, and C-H. These oxygen/nitrogen-containing groups have a good affinity to form strong interaction and coordination bonds with Fe^{3+} ions by donating electron pairs to the metal ions, resulting in the fluorescence quenching effect [11, 49–51]. The findings indicated that CDs and Fe-CDs have great potential as fluorescent probes for rapid, low-cost, and accurate detection of DFS at various concentrations. In addition, the relationship between the FL intensity of Fe-CDs with various concentrations of DFS was evaluated (Fig. 11b). Noteworthy, the good linearity relation was obtained between the FL intensity of Fe-CDs with the different concentrations of DFS in the range of 5-300 µM. In this case, the linear regression correlation for DFS could be described with the equation of F/F_0 = -0.0018 C_{DFS} + 0.0227, and the correlation coefficient was R^2 = 0.9970. Also, the LOD was calculated to be 0.12 µM ($3\sigma/K$). Actually, adding Fe^{3+} to CDs improved the LOD of as-prepared CDs. The results suggest that the as-prepared Fe-CDs is superior fluorescent probe and has great prospects for DFS detection in different systems.

Conclusions

In this work, the CDs and Fe-CDs were prepared through a facile, rapid, low-cost, and one-step microwave heating approach without any further modification for the detection of various concentrations of DFS in the broad range of 5-300 µM. The as-prepared CDs possessed excellent characteristics, including appropriate size and morphology, good water solubility, various functional groups, and outstanding stability towards different environmental conditions. In addition, the FL intensity of the synthesized CDs and Fe-CDs showed a linear response with the different concentrations of DFS over the wide range of 5-300 µM with the LOD of 2.33 and 0.12 µM, respectively. Furthermore, the as-prepared CDs can be applied as a fluorescent probe for detection of a wide range of DFS on the test papers (NCs) and different real samples. These results demonstrated that the sensing system is a fast, powerful, selective and efficient approach for detecting a wide range of different concentrations of DFS in various environments.

Declarations

Ethical Approval This manuscript does not contain any studies with human and/ or animals performed by any of the authors.

Conflict of interest The authors declare that they have no any competing interest.

Availability of data and materials All data related to this publication are made available in the article.

References

1. P. Namdari, B. Negahdari, and A. Eatemadi (2017). *Biomed. Pharmacother*. **87**, 209-222. https://doi.org/10.1016/j.biopha.2016.12.108.

2. Z. Peng, X. Han, S. Li, A.O. Al-Youbi, A.S. Bashammakh, M.S. El-Shahawi, and R. M. Leblanc (2017). *Coord. Chem. Rev*. **343**, 256-277. https://doi.org/10.1016/j.ccr.2017.06.001.

3. Q. Wang, X. Huang, Y. Long, X. Wang, H. Zhang, R. Zhu, L. Liang, P. Teng, and H. Zheng (2013). *Carbon*. **59**, 192-199. https://doi.org/10.1016/j.carbon.2013.03.009.

4. T. Madrakian, S. Maleki, S. Gilak, and A. Afkhami (2017). *Sens. Actuators B Chem*. **247**, 428-435. https://doi.org/10.1016/j.snb.2017.03.071.

5. F. Wang, P. Chen, Y. Feng, Z. Xie, Y. Liu, Y. Su, Q. Zhang, Y. Wang, K. Yao, and W. Lv (2017). *Appl. Catal. B*. **207**, 103-113. https://doi.org/10.1016/j.apcatb.2017.02.024.

6. J. Zhang, L. Dong, and S.H. Yu (2015). *Sci. Bull*. **60**, 785-791. https://doi.org/10.1007/s11434-015-0764-5.

7. R. Malik, S. Lata, U. Soni, P. Rani, and R. S. Malik (2020). *Electrochim. Acta*. **364**, 137281. https://doi.org/10.1016/j.electacta.2020.137281.

8. P. Devi, S. Saini, and K.H. Kim (2019). *Biosens. Bioelectron*. **141**, 111158. https://doi.org/10.1016/j.bios.2019.02.059.

9. X. Hu, Y. Li, Y. Xu, Z. Gan, X. Zou, J. Shi, X. Huang, Z. Li, and Y. Li (2021). *Food Chem*. **339**, 127775. https://doi.org/10.1016/j.foodchem.2020.127775.

10. D. L. Zhao, and T.S. Chung (2018). *Water Res*. **147**, 43-49. https://doi.org/10.1016/j.watres.2018.09.040.

11. S. Zhao, X. Song, X. Chai, P. Zhao, H. He, and Z. Liu (2020). *J. Clean. Prod*. **263**, 121561. https://doi.org/10.1016/j.jclepro.2020.121561.

12. Y. Zhao, S. Zou, D. Huo, C. Hou, M. Yang, J. Li, and M. Bian (2019). *Anal. Chim. Acta*. **1047**, 179-187. https://doi.org/10.1016/j.aca.2018.10.005.

13. J. Guo, W. Lu, H. Zhang, Y. Meng, F. Du, S. Shuang, and C. Dong (2021). *Sens. Actuators B Chem*. **330**, 129360. https://doi.org/10.1016/j.snb.2020.129360.

14. X. Zhang, Y. Ren, Z. Ji, and J. Fan (2020). *J. Mol. Liq*. **311**, 113278. https://doi.org/10.1016/j.molliq.2020.113278.

15. X. Miao, X. Yan, D. Qu, D. Li, F.F. Tao, and Z. Sun (2017). *ACS Appl. Mater. Interfaces*. **9**, 18549-18556. https://doi.org/10.1021/acsami.7b04514.

16. O.K. Okoth, K. Yan, J. Feng, and J. Zhang (2018). *Sens. Actuators B Chem*. **256**, 334-341. https://doi.org/10.1016/j.snb.2017.10.089.

17. M. Goodarzian, M.A. Khalilzade, F. Karimi, V. K. Gupta, M. Keyvanfard, H. Bagheri, and M. Fouladgar (2014). *J. Mol. Liq*. **197**, 114-119. https://doi.org/10.1016/j.molliq.2014.04.037.

18. B. Klencsár, L. Balcaen, F. Cuyckens, F. Lynen, and F. Vanhaecke (2017). *Anal. Chim. Acta*. **974**, 43-53. https://doi.org/10.1016/j.aca.2017.04.030.

19. G. Daniele, M. Fieu, S. Joachim, A. James-Casas, S. Andres, P. Baudoin, M. Bonnard, I. Bonnard, A. Geffard, and E. Vulliet (2016). *Talanta*. **155**, 1-7. https://doi.org/10.1016/j.talanta.2016.04.016.

20. B. Yilmaz, and U. Ciltas (2015). *J. Pharm. Anal*. **5**, 153-160. https://doi.org/10.1016/j.jpha.2014.10.005.

21. X. Miao, D. Qu, D. Yang, B. Nie, Y. Zhao, H. Fan, and Z. Sun (2018). *Adv. Mater*. **30**, 1704740. https://doi.org/10.1002/adma.201704740.

22. Y. Yang, Z. Liu, D. Chen, B. Gu, B. Gao, Z. Wang, Q. Guo, and G. Wang (2021). *J. Photochem. Photobiol. A*. **405**, 112977. https://doi.org/10.1016/j.jphotochem.2020.112977.

23. J.B. Wu, M.L. Lin, X. Cong, H.N. Liu, and P.H. Tan (2018). *Chem. Soc. Rev*. **47**, 1822-1873. https://doi.org/10.1039/C6CS00915H.

24. K. N. Kudin, B. Ozbas, H. C. Schniepp, R. K. Prud'Homme, I. A. Aksay, and R. Car (2008). *Nano lett*. **8**, 36-41. https://doi.org/10.1021/nl071822y.

25. C. Zhu, C. Liu, Y. Zhou, Y. Fu, S. Guo, H. Li, S. Zhao, H. Huang, Y. Liu, and Z. Kang (2017). *Appl. Catal. B*. **216**, 114-121. https://doi.org/10.1016/j.apcatb.2017.05.049.

26. S. Liu, J. Tian, L. Wang, Y. Zhang, X. Qin, Y. Luo, A. M. Asiri, A. O. Al-Youbi, and X. Sun (2012). *Adv. Mater*. **24**, 2037-2041. https://doi.org/10.1002/adma.201200164.

27. L. Shi, X. Li, Y. Li, X. Wen, J. Li, M.M. Choi, C. Dong, and S. Shuang (2015). *Sens. Actuators B Chem*. **210**, 533-541. https://doi.org/10.1016/j.snb.2014.12.097.

28. J. Yue, L. Li, L. Cao, M. Zan, D. Yang, Z. Wang, Z. Chang, Q. Mei, P. Miao, and W.F. Dong (2019). *ACS Appl. Mater. Interfaces*. **11**, 44566-44572. https://doi.org/10.1021/acsami.9b13737.

29. D. B. Gunjal, Y. M. Gurav, A. H. Gore, V. M. Naik, R. D. Waghmare, C. S. Patil, D. Sohn, P. V. Anbhule, R. V. Shejwal, and G. B. Kolekar (2019). *Opt. Mater*. **98**, 109484. https://doi.org/10.1016/j.optmat.2019.109484.

30. S. Huang, E. Yang, J. Yao, Y. Liu, and Q. Xiao (2018). *Anal. Chim. Acta*. **1035**, 192-202. https://doi.org/10.1016/j.aca.2018.06.051.

31. K. Zhao, X. Zheng, H. Zhang, M. Xu, S. Wang, Q. Yang, and C. Xiong (2019). *J. Alloys Compd*. **793**, 613-619. https://doi.org/10.1016/j.jallcom.2019.04.146.

32. J. Zhou, X. Shan, J. Ma, Y. Gu, Z. Qian, J. Chen, and H. Feng (2014). *RSC Adv*. **4**, 5465-5468. https://doi.org/10.1039/C3RA45294H.

33. X.C. Liang, S. Chen, J. Gao, H. Zhang, Y. Wang, J.H. Wang, and L. Feng (2018). *Sens. Actuators B Chem*. **265**, 293-301. https://doi.org/10.1016/j.snb.2018.01.182.

34. L. Zhang, D. Peng, R.P. Liang, and J.D. Qiu (2018). *Trends Analyt Chem*. **102**, 280-289. https://doi.org/10.1016/j.trac.2018.02.010.

35. Y. Wang, S.H. Kim, and L. Feng (2015). *Anal. Chim. Acta*. **890**, 134-142. https://doi.org/10.1016/j.aca.2015.07.051.

36. M. Xue, L. Zhang, M. Zou, C. Lan, Z. Zhan, and S. Zhao (2015). *Sens. Actuators B Chem*. **219**, 50-56. https://doi.org/10.1016/j.snb.2015.05.021.

37. X. Li, S. Zhang, S. A. Kulinich, Y. Liu, and H. Zeng (2014). *Sci. Rep.* **4**, 4976. https://doi/10.1038/srep04976.

38. R. Vaz, J. Bettini, J. G. F. Júnior, E. D. S. Lima, W. G. Botero, J. C. C. Santos, and M. A. Schiavon (2017). *J. Photochem. Photobiol. A*. **346**, 502-511. https://doi.org/10.1016/j.jphotochem.2017.06.047.

39. B. Zhi, M. J. Gallagher, B. P. Frank, T. Y. Lyons, T. A. Qiu, J. Da, A. C. Mensch, R. J. Hamers, Z. Rosenzweig, and D. H. Fairbrother (2018). *Carbon*. **129**, 438-449. https://doi.org/10.1016/j.carbon.2017.12.004.

40. H. Li, X. He, Z. Kang, H. Huang, Y. Liu, J. Liu, S. Lian, C. H. A. Tsang, X. Yang, and S. T. Lee (2010). *Angew. Chem. Int. Ed*. **49**, 4430-4434. https://doi.org/10.1002/anie.200906154.

41. K. Wang, F. Guan, H. Li, M. Li, H. Feng, and H. Fan (2015). *RSC Adv*. **5**, 20511-20515. https://doi.org/10.1039/C4RA15433A.

42. R. Zhang, and W. Chen (2014). *Biosens. Bioelectron*. **55**, 83-90. https://doi.org/10.1016/j.bios.2013.11.074.

43. Q. Xu, J. Wei, J. Wang, Y. Liu, N. Li, Y. Chen, C. Gao, W. Zhang, and T. S. Sreeprased (2016). *RSC Adv*. **6**, 28745-28750. https://doi.org/10.1039/C5RA27658F.

44. L. S. Walekar, M. Zheng, L. Zheng, and M. Long (2019). *MICROCHIM ACTA*. **186**, 1-9. https://doi.org/10.1007/s00604-019-3532-4.

45. X. An, S. Zhuo, P. Zhang, and C. Zhu (2015). *RSC Adv*. **5**, 19853-19858. https://doi.org/10.1039/C4RA16456C.

46. S. Nazerdeylami, J. B. Ghasemi, G. M. Ziarani, A. Amiri, and A. Badiei (2021). *J. Mol. Liq*. **336**, 116104. https://doi.org/10.1016/j.molliq.2021.116104.

47. J. Hou, J. Yan, Q. Zhao, Y. Li, H. Ding, and L. Ding (2013). *Nanoscale*. **5**, 9558-9561. https://doi.org/10.1039/C3NR03444E.

48. Z. L. Wu, P. Zhang, M. X. Gao, C. F. Liu, W. Wang, F. Leng, and C. Z. Huang (2013). *J. Mater. Chem. B*. **1**, 2868-2873. https://doi.org/10.1039/C3TB20418A.

49. D. Zhu, S. Zhuo, C. Zhu, P. Zhang, and W. Shen (2019). *Anal. Methods*. **11**, 2663-2668. https://doi.org/10.1039/C9AY00342H.

50. S. Zhuo, Y. Guan, H. Li, J. Fang, P. Zhang, J. Du, and C. Zhu (2019). *Analyst*. **144**, 656-662. https://doi.org/10.1039/C8AN01741G

51. P. Song, L. Zhang, H. Long, M. Meng, T. Liu, Y. Yin, and R. Xi (2017). *RSC Adv.* **7**, 28637-28646. https://doi.org/10.1039/C7RA04122E.
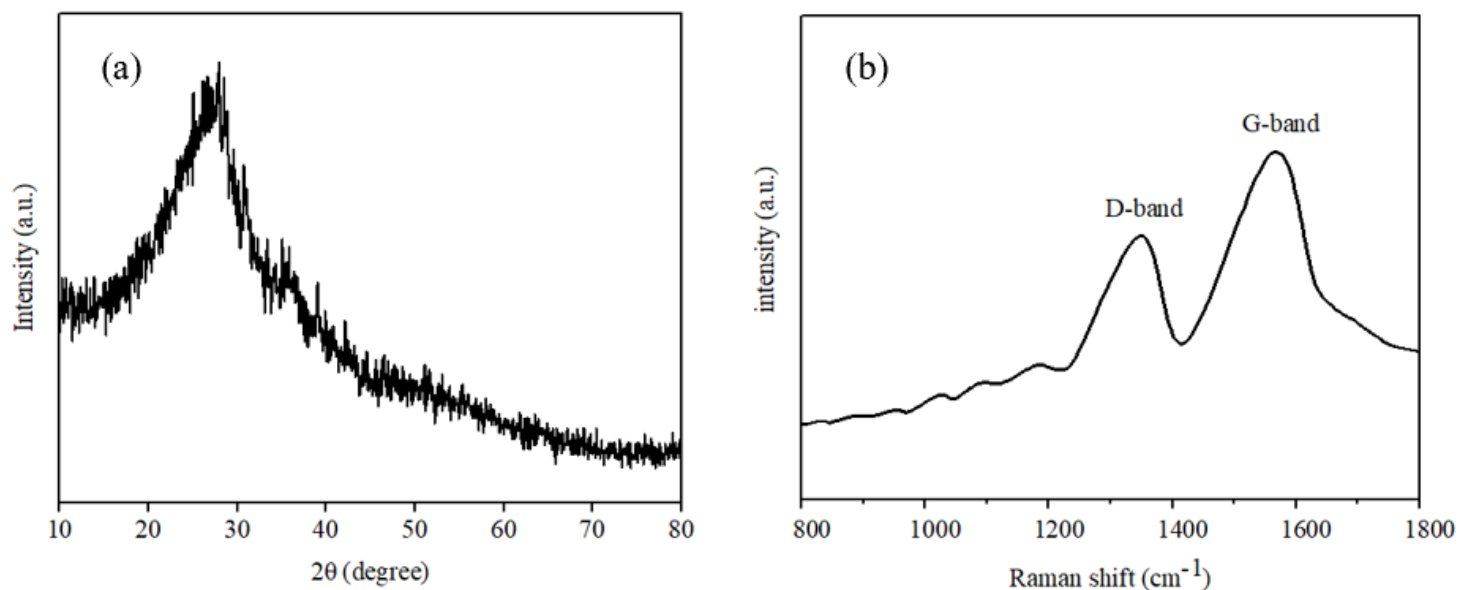
Figures

Figure 1

(a) The XRD pattern, and (b) Raman spectrum of as-prepared CDs.
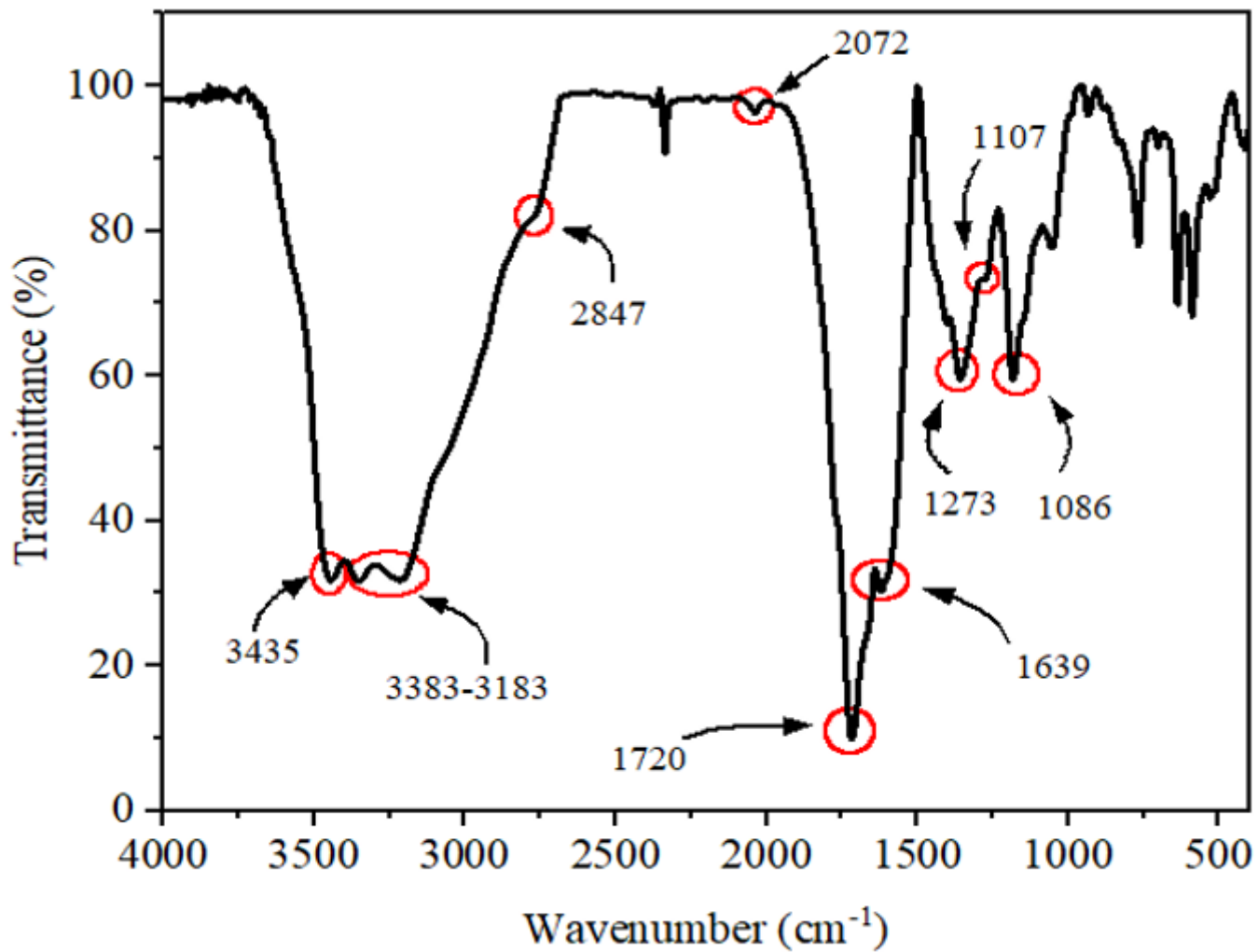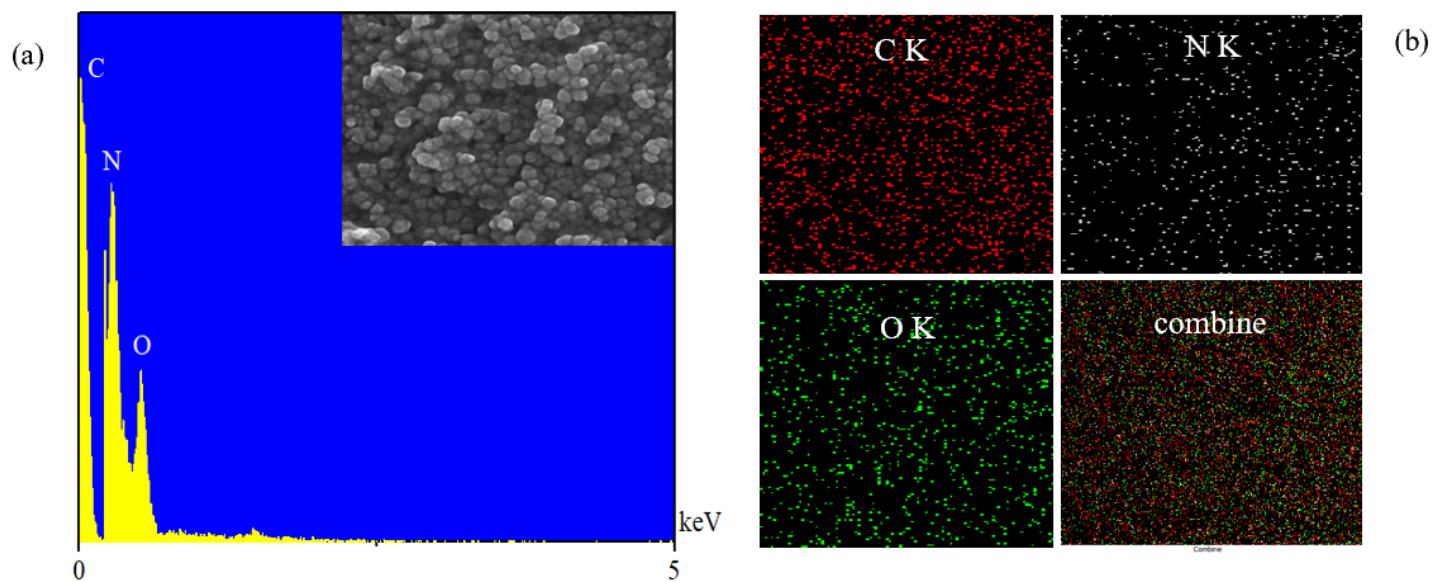
Figure 2

The FTIR spectrum of CDs.

Figure 3
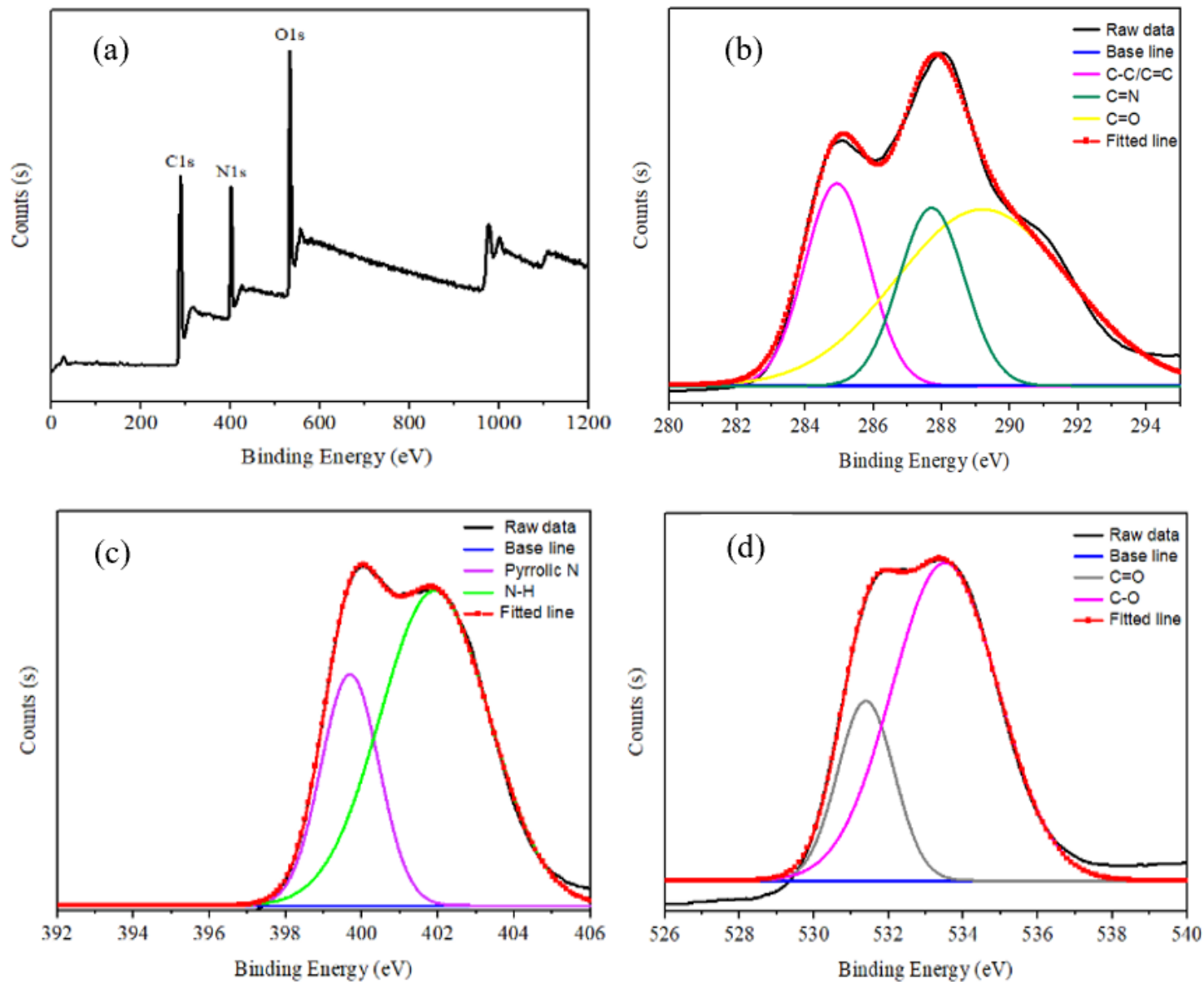
(a) The SEM image, EDS spectrum, and (b) Elemental mapping of as-prepared CDs.

Figure 4

(a) The XPS survey, and the high resolution of (b) C1s, (c) N1s, and (d) O1s spectra of the as-prepared CDs.
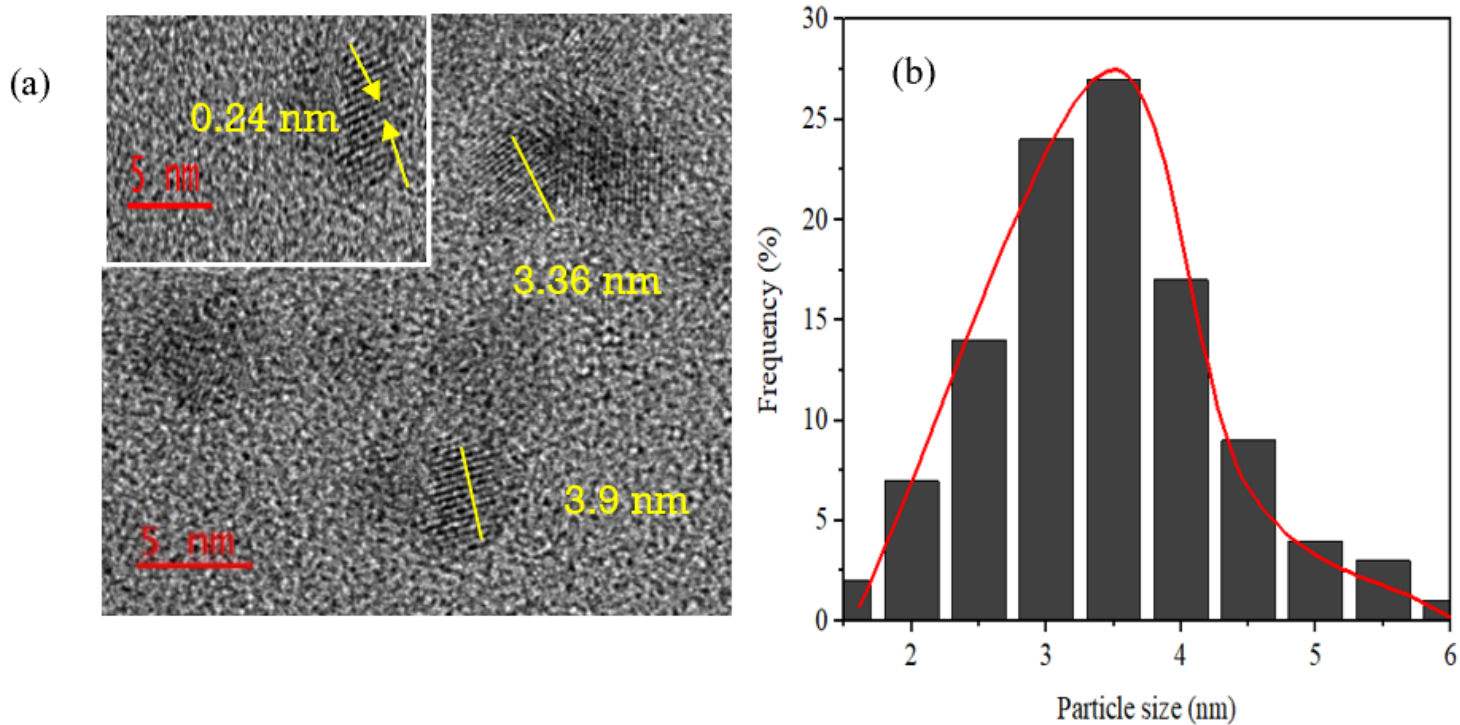
Figure 5

(a) The HRTEM images of as-prepared CDs; inset of (a) shows crystalline lattice spacing of CDs, (b) Displays a histogram for the size distribution of particles.
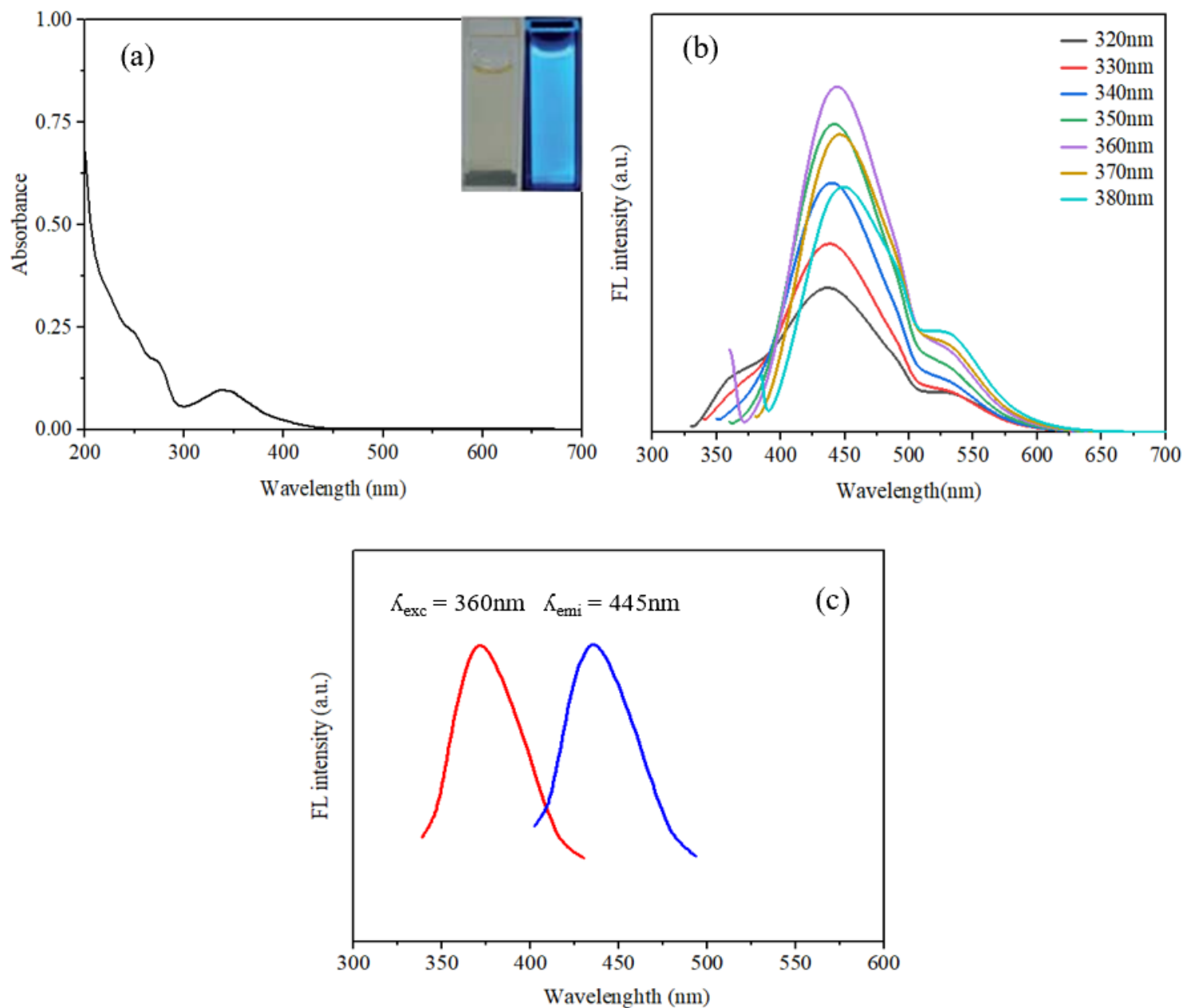
Figure 6

(a) The absorption spectra of as-prepared CDs; inset of (a) shows the photographs of CDs in aqueous solution under visible light (left) and 360 nm UV light (right), (b) The emission spectra of CDs under different excitation wavelengths, and (c) The optimal excitation and emission wavelength for as-prepared CDs.
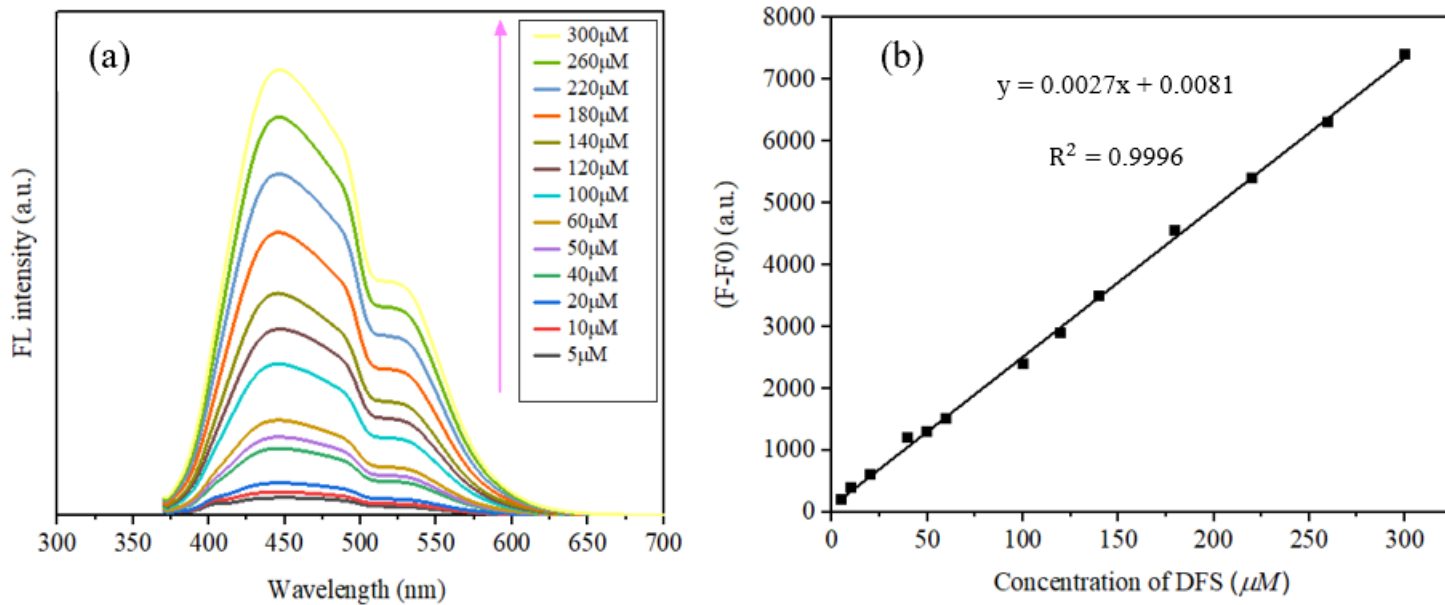
Figure 7

(a) FL spectra of as-prepared CDs in the presence of different concentrations of DFS and (b) The linear relationship between the FL intensity of CDs with DFS in the wide range of concentrations from 5 to 300 μM.
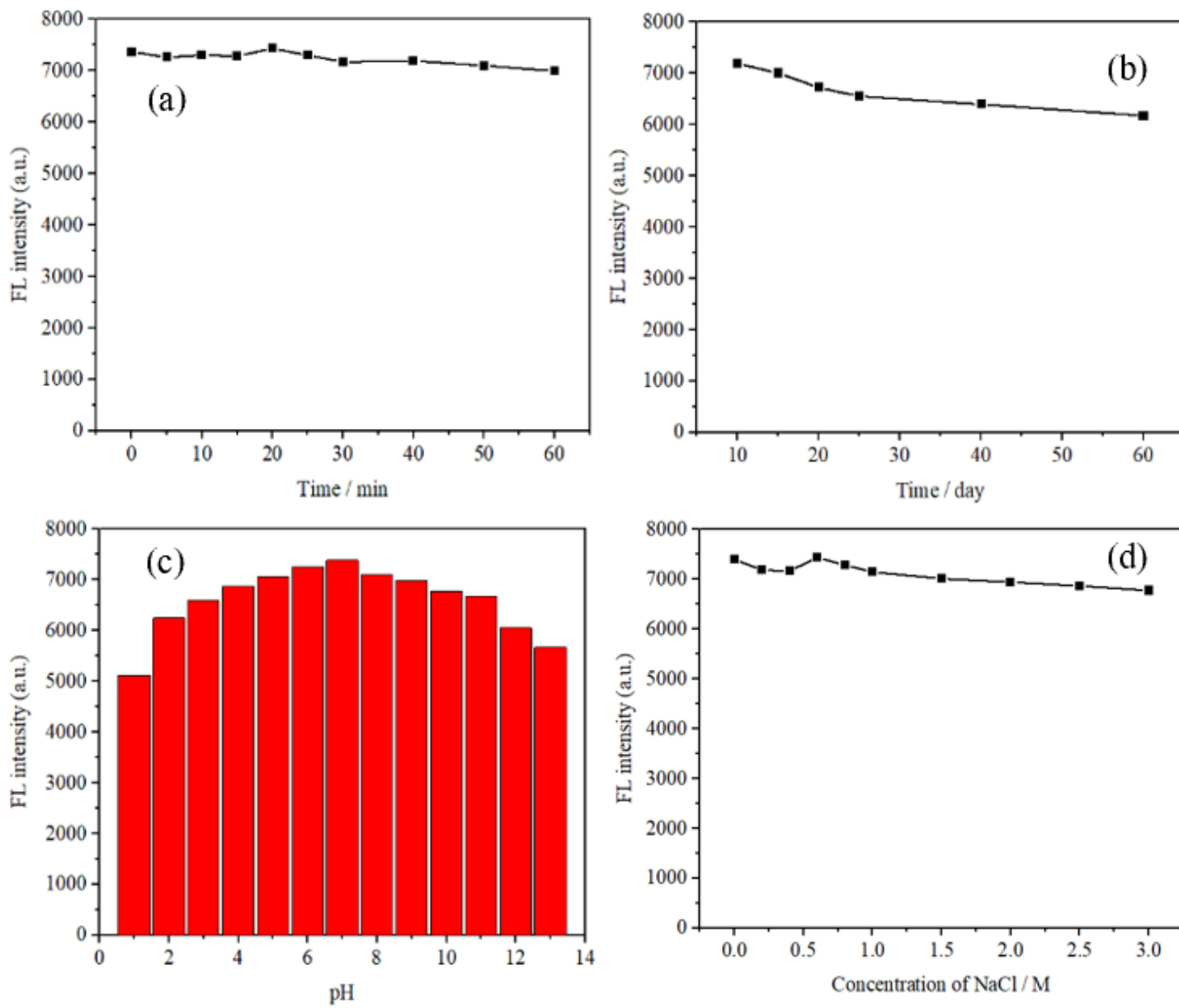
Figure 8

Stability performance of the FL intensity of CDs (a) Under ultraviolet light at different irradiation times, (b) Diverse storage times, (c) Various pH values, and (d) Different concentrations of NaCl ($_{exc}$ = 360 nm, $_{emi}$ = 445 nm; and C_{CQDs} = 5 µg.ml^{-1}).

Figure 9

The photographs of CDs-based test papers with diverse concentrations of DFS under a UV lamp (The concentration of DFS from left to right was 0, 60, 140, 260, and 300 µM, respectively).
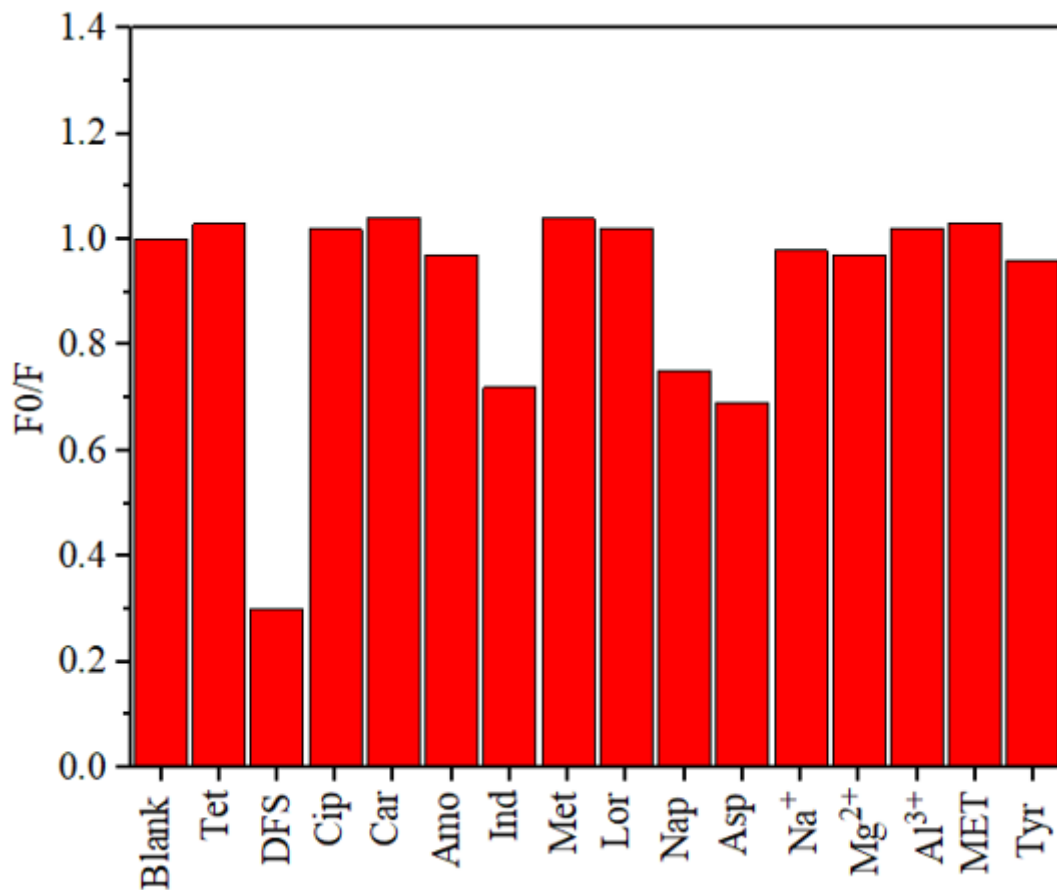

Figure 10

The selectivity of as-prepared CDs solution after addition of different drugs, metal ions, and amino acids (the concentration of all interferences were 100 µM).
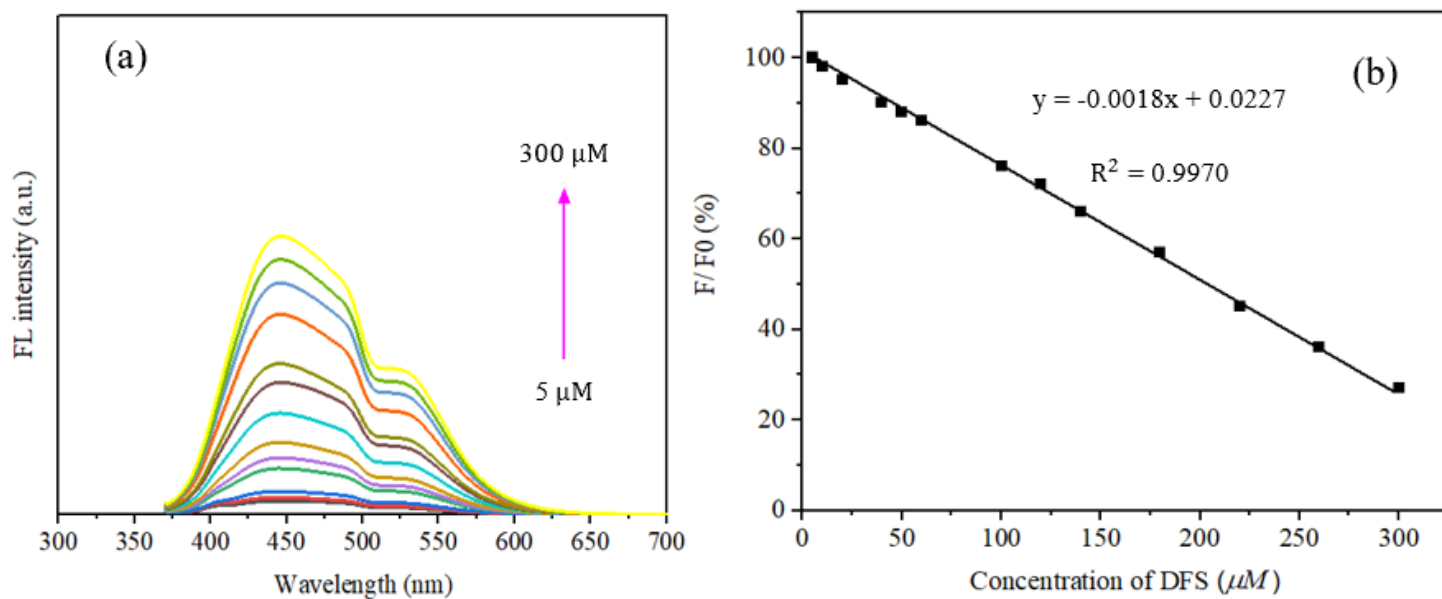
Figure 11

(a) FL spectra of as-prepared Fe-CDs in the presence of different concentrations of DFS and (b) The linear relationship between the FL intensity of Fe-CDs with DFS in the wide range of concentrations from 5 to 300 μM.

Supplementary Files

This is a list of supplementary files associated with this preprint. Click to download.

- Graphicalabstract.png